Spontaneous wrinkle branching by gradient stiffness

Yong Ni,* Dong Yang, and Linghui He

Department of Modern Mechanics, CAS Key Laboratory of Mechanical Behavior and Design of Materials, University of Science and Technology of China, Hefei, Anhui 230026, People's Republic of China

(Received 18 July 2012; published 24 September 2012)

The concept of coherency loss is proposed to understand wrinkle branching as a pathway toward hierarchical wrinkling pattern formation in a compressed film-substrate system with gradient stiffness of the film or substrate. A simple model indicates that the wrinkle branching arises when the characteristic length of the stiffness inhomogeneity zone is larger than the coherency persistent length, which depends on the amplitude of the stiffness inhomogeneity. Numerical simulations of nonlinear wrinkles based on the model of the Föppl–von Kármán plate on compliant substrates show how regulating the size and amplitude of the stiffness inhomogeneities results in branched wrinkles in striking agreement with the existing observations. The paper reveals the origin of such kinds of branched wrinkles and may provide a guideline for controllable hierarchical wrinkles by patterning the stiffness gradient.

DOI: 10.1103/PhysRevE.86.031604 PACS number(s): 68.08.−p, 62.20.mq, 68.55.−a, 64.75.Yz

I. INTRODUCTION

Elastic-energy-driven hierarchical pattern formation has been found in martensitic twinning [1–4], undulations in the meniscus of smectic membranes [5], film blistering [6–8], folding [9–11], and wrinkles [12–16]. Formation of these patterns has been explained on the basis of minimization of nonconvex elastic strain energy and interface energy from a strain gradient contribution. In the twins near an interface between austenite and twinned martensite, the classic theory of domains predicts parallel twins of constant width when the austenite and martensite have the same stiffness [17,18] and twin branching when their stiffnesses are significantly different [1]. The hierarchical twinned microstructure may be a manifestation as the coexistence of twins with different widths due to twin branching. The analogy between the hierarchical twin pattern and the buckling pattern in a confined film has been drawn wherein both of them can be classified into a multiscale variational problem for an extended Ginzburg-Landau functional including gradient and nonlocal terms [7]. However, due to the rare observation of the hierarchical twin pattern, it is still unclear that the formation of such kinds of twin patterns is solely dominated by energy minimization or just local minima prevented by dynamic inaccessibility [1]. Recently, hierarchical wrinkling patterns have been observed in a film under uncompressed boundary confinement [12–14] or in solvent-induced wrinkling of multilayer systems [15]. This provides another platform to revisit the hierarchical pattern driven by elastic energy. In addition, the hierarchical wrinkling pattern as a tunable microstructured surface is attracting more and more interest in applications of flexible electronics [19], artificial skin [20], and cell mechanosensitivity [15].

We note that the reported hierarchical wrinkling patterns are closely related to the stiffness inhomogeneities of the film or the substrate, and the coexistence of the straight wrinkles with different wavelengths is topologically like a dislocated configuration due to coherency loss. In this paper, we propose a model based on energy minimization to demonstrate that the coherency loss in hierarchical wrinkles induced by gradient stiffness can be viewed as a mechanism of the wrinkle-branching instability, which is a pathway toward the formation of the hierarchical wrinkling pattern. Nonlinear wrinkling simulation based on the continuum modeling for an elastically heterogeneous Föppl–von Kármán (FvK) plate on the compliant substrate and a homogeneous FvK plate on the viscoelastic substrate is also developed. The numerical results have confirmed the critical condition for the wrinkle-branching instability derived in the simple model and have revealed how the hierarchical wrinkle forms during the buckling process.

II. THEORETIC MODEL OF WRINKLE BRANCHING

Previous papers have shown that a film of thickness h on a semi-infinite compliant substrate under a uniaxial compression ε_{pre} may buckle with straight wrinkle morphology, which is determined by the optimal release of the elastic energies in the film and substrate [21–24]. In the approximation of the sinusoidal wrinkling mode, following the analysis given by the reference in Ref. [24], the shear stress at the film-substrate interface can be neglectable, and it leads to uniform membrane stress and membrane strain. If the out-of-plane deflection in the film is $u_3^f = A\ cos(2\pi x/\lambda)$ with A and λ as the amplitude and wavelength of the wrinkle, respectively, the in-plane displacement fields can be obtained as $u_1^f = \frac{\pi A^2}{4\lambda} sin(4\pi x/\lambda)$ and $u_2^f = 0$ according to the condition of uniform membrane strains, wherein the membrane strain and stress are $\varepsilon_{11}^f = \frac{\pi^2 A^2}{\lambda^2} - \varepsilon_{\text{pre}}$, $\varepsilon_{22}^f = 0$, $N_{11}^f = \bar{E}_f \varepsilon_{11}^f$, and $N_{22}^f = v_f \bar{E}_f \varepsilon_{11}^f$, respectively. The elastic energy per unit area in the wrinkled film, including the bending and stretching terms, is then expressed as $\frac{h^3 \bar{E}_f \pi^4 A^2}{3\lambda^4} + \frac{1}{2} N_{11}^f \varepsilon_{11}^f$. The elastic energy per unit area in the substrate is $U^{\text{sub}} = \frac{1}{\lambda}\int_0^\lambda \frac{1}{2} T_3 u_3^f dx_1 = \frac{\pi \bar{E}_s A^2}{4\lambda}$ by using the Gauss divergence theorem, where $T_3 = \frac{\pi}{\lambda}\bar{E}_s u_3^f$ is given by the Green's function method. The total elastic energy in the film-substrate system minimizes at $A = 0$ as $\varepsilon_{\text{pre}} < \varepsilon_c = (3\bar{E}_s/\bar{E}_f)^{2/3}/4$, whereas, at $A(\lambda) = \frac{\lambda}{\pi}\sqrt{\varepsilon_{\text{pre}} - (\frac{\pi^2 h^2}{3\lambda^2} + \frac{\lambda \bar{E}_s}{4\pi h \bar{E}_f})}$, it minimizes as $\varepsilon_{\text{pre}} > \varepsilon_c$. Finally, the total elastic energy per unit area in the

*Email address: yni@ustc.edu.cn

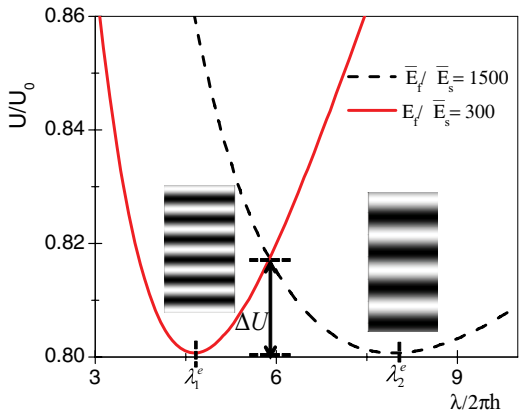

FIG. 1. (Color online) The reduced total elastic energy as a function of the reduced wavelength $\lambda/2\pi h$ under different values of the film-substrate modulus ratio.

wrinkled state has the form in terms of $\varepsilon_{\rm pre}$ and λ,

$$\frac{U}{U_0} = 1 - \left[1 - \left(\frac{\pi^2 h^2}{3\lambda^2} + \frac{\lambda \bar{E}_s}{4\pi h \bar{E}_f}\right)/\varepsilon_{\rm pre}\right]^2, \qquad (1)$$

with $U_0 = \frac{1}{2} h \bar{E}_f \varepsilon_{\rm pre}^2$ and $\bar{E}_{f,s} = E_{f,s}/(1-\upsilon_{f,s}^2)$, where $E_{f,s}$ and $\upsilon_{f,s}$ are the Young's modulus and the Poisson's ratio of the film or substrate, respectively. The plot in Fig. 1 shows that, if both the film and the substrate are elastically homogeneous, i.e., $\bar{E}_f^{(1)}/\bar{E}_s = 300$ above a critical buckling strain $\varepsilon_{c1} = (3\bar{E}_s/\bar{E}_f^{(1)})^{2/3}/4$, the total elastic energy has a minimum at $\lambda = \lambda_1^e$ with $\lambda_1^e/2\pi h = (\bar{E}_f^{(1)}/3\bar{E}_s)^{1/3}$ and the amplitude of the equilibrium out of displacement $A/h = (\varepsilon_{\rm pre}/\varepsilon_{c1} - 1)^{1/2}$. If the modulus ratio of the film and the substrate changes, the minimum of the elastic energy shifts to another value λ_2^e as shown in Fig. 1. The plot of the elastic energy U per unit area at $\bar{E}_f^{(2)}/\bar{E}_s = 1500$ plus a constant $U_{\rm min}(\lambda_1^e) - U_{\rm min}(\lambda_2^e)$ with respect to λ is added in Fig. 1. The combination of two curves in Fig. 1 shows that, if the modulus ratio between the film and the substrate is positionally dependent, the elastic energy is split into a double well or multiwell, which indicates the possibility of coexistence of the straight wrinkles with different wavelengths. Figure 2 shows two typical coexistent wrinkling configurations. Figure 2(a) is the coherent wrinkle where both the wrinkles deviate from each equilibrium configuration with its wavelength matched with an intermediate value $\lambda_1^e < \lambda^e < \lambda_2^e$. Figure 2(b) is the coherency-loss wrinkle where there is a dislocated boundary bridging the wrinkle of its wavelength λ_1^e

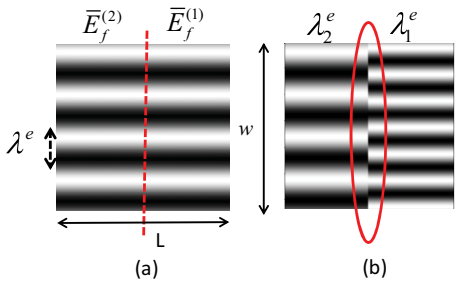

FIG. 2. (Color online) Sketches of two typical coexistent wrinkling configurations with stiff inhomogeneity.

and the wrinkle of its wavelength λ_2^e. The energy change in the configuration with respect to the case of the uniform modulus ratio in Fig. 2(a) is $\Delta U\ Lw$ with $\Delta U = U(\lambda^e)$, whereas, it is $\gamma_l w$ for the configuration in Fig. 2(b), where γ_l is the effective line energy per unit length along the dislocated boundary, and ΔU is the energy increase per unit area due to the coherency as shown in Fig. 1. The coherent wrinkle configuration has a lower free energy when $\Delta U\ Lw < \gamma_l w$. This defines a coherency persistent length $L_c = \gamma_l/\Delta U$.

Using the two-well parabolic approximation, the elastic energy curves in Fig. 2 can be approximately fitted into $U \approx B(\lambda - \lambda_1^e)^2(\lambda - \lambda_2^e)^2$ where B is a factor dependent on the value of the uniaxial compression. When the wrinkle branching occurs, there is a wrinkle wavelength gradient as well as additional film bending and substrate distortion energies localized at the transition boundary from the wrinkle of its wavelength λ_1^e to the wrinkle of its wavelength λ_2^e. Following the Gibbs's description, if we assume the wrinkle-branched system as two phases separated by the boundary, the excess energy at the sharp boundary is defined as the effective line energy, which is determined by direct numerical calculation. It can also be estimated according to classic diffuse interface theory [25]. Using the theory, the equilibrium wrinkle wavelength gradient profile is determined by minimizing the elastic energy plus the contribution of the gradient term with respect to $\lambda(x)$ under the boundary condition $\lambda(x \to \infty) = \lambda_2^e$, $\lambda(x \to -\infty) = \lambda_1^e$. If we introduce a long-range order parameter $\eta = \frac{\lambda - \lambda_1^e}{\lambda_2^e - \lambda_1^e}$ $(0 \leqslant \eta \leqslant 1)$, the total elastic energy in the wrinkle-branched system with respect to η is assumed to have the form $U^{\rm tot} = \int_{-\infty}^{+\infty} w[16\ \Delta U \eta^2(1-\eta)^2 + \beta(\frac{\partial \eta}{\partial x})^2]dx$ with $\Delta U = B(\lambda_2^e - \lambda_1^e)^4/16$ at $\lambda^e \sim \frac{(\lambda_2^e + \lambda_1^e)}{2}$. $\beta(\frac{\partial \eta}{\partial x})^2$ with β as the gradient coefficient, is the gradient energy term. The solution $\eta(x) = \frac{1}{2}[1 - \tanh(-x/l)]$ with $l = \sqrt{\beta/\Delta U}/2$ is obtained by solving the equation $2\beta \frac{d^2\eta}{dx^2} = \frac{dU}{d\eta}$ from $\delta U^{\rm tot}(\eta)/\delta\eta = 0$ under the boundary condition $\eta(x \to \infty) = 1$, $\eta(x \to -\infty) = 0$. The calculated equilibrium line energy γ_l is calculated as $\gamma_l = \frac{4}{3}\sqrt{\beta\ \Delta U}$ through $\gamma_l = \int_{-\infty}^{+\infty} 2\beta(\frac{\partial \eta}{\partial x})^2 dx$. Substituting the expression of $\gamma_l \sim \sqrt{\beta\ \Delta U}$ and $\Delta U \sim B(\lambda_2^e - \lambda_1^e)^4$ with $\lambda_i^e/2\pi h = (\bar{E}_f^{(i)}/3\bar{E}_s)^{1/3}$ into $L_c = \gamma_l/\Delta U$, the coherency persistent length, thus, has the form as a function of $\alpha = \bar{E}_f^{(1)}/\bar{E}_f^{(2)}$ $(\bar{E}_f^{(1)} \leqslant \bar{E}_f^{(2)})$,

$$L_c = \frac{C}{(1 - \alpha^{1/3})^2}, \qquad (2)$$

where $C \approx \sqrt{\beta/B}(3\bar{E}_s/\bar{E}_f^{(2)})^{1/3}/(2\pi h)^2$ is a constant. This indicates that there is a wrinkle-branching instability when the characteristic length of the stiffness inhomogeneity zone satisfies the critical condition $L > L_c$. The coherency persistent length increases as the increase in α, and it is divergent as $\alpha \to 1$ where the stiffness inhomogeneity in the film vanishes. If the stiffness inhomogeneity is in the substrate, it also changes the film-substrate modulus ratio and results in the coexistence of a different wrinkle wavelength $\lambda_i^e/2\pi h = (\bar{E}_f/3\bar{E}_s^{(i)})^{1/3}$, therefore, a similar result in Eq. (2) is still valid after α is replaced by $\bar{E}_s^{(2)}/\bar{E}_s^{(1)}$ $(\bar{E}_s^{(2)} \leqslant \bar{E}_s^{(1)})$ and C is replaced by $\sqrt{\beta/B}(3\bar{E}_s^{(2)}/\bar{E}_f)^{2/3}/(2\pi h)^2$. Apparently, small values of α corresponding to strong stiffness inhomogeneity and a large

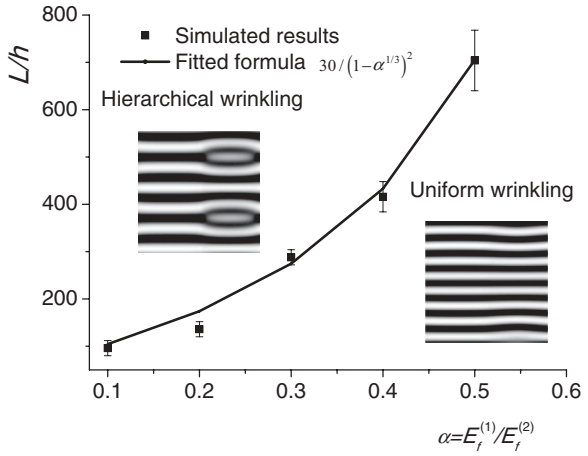

FIG. 3. The calculated phase diagram for the wrinkle-branching morphology of the film-substrate system with the stiffness gradient constructed in the space with L and α as the coordinates.

value of L facilitate the wrinkle-branching instability. There is a phase diagram shown in Fig. 3 constructed in the space with L and α as the coordinates for the morphology of the film-substrate system under the given uniaxial compression $\varepsilon_{\text{pre}} > \varepsilon_c$ either in a uniform straight wrinkle state or in a wrinkle-branching state. By using a continuum model and simulation developed in the following section without imposing any *ad hoc* constraints on the possible buckling geometry, the transition from the uniform straight wrinkle state to the wrinkle-branching state can be identified by tracking the configuration instability of the film-substrate system for various cases with different values of these L's and α's. The plots of L_c/h with respect to α in Fig. 3 show that the numerical solution can be well fitted by the formula in Eq. (2). The consistency indicates that the simple model captures the main feature of the wrinkle branching induced by stiffness gradient. The result in Fig. 3 can further be applied to design the hierarchical wrinkling pattern by regulating the values of L and α.

III. NUMERICAL SIMULATIONS OF HIERARCHICAL WRINKLES

In this section, we performed numerical simulations for nonlinear wrinkles based on the modified continuum model with the consideration of stiffness inhomogeneities in the film or substrate [24,26,27]. Two film-substrate systems are investigated, respectively. One is a film with stiffness inhomogeneity on a homogeneous compliant substrate. The other is an elastically homogeneous film on a viscoelastic substrate with stiffness inhomogeneity induced by the interplay between the substrate viscoelasticity and the diffusion process in the film. In the continuum model, the film with an eigenstrain $\varepsilon^0_{\alpha\beta}$ is taken as the FvK plate [28], the elastic strain in the film can be expressed by the middle-plane displacement $\mathbf{u}^f = (u_\alpha, \zeta)$,

$$\varepsilon^e_{\alpha\beta} = \tfrac{1}{2}(u_{\alpha,\beta} + u_{\beta,\alpha}) + \tfrac{1}{2}\zeta_{,\alpha}\zeta_{,\beta} - \varepsilon^0_{\alpha\beta} - x_3\zeta_{,\alpha\beta}. \tag{3}$$

The total elastic strain energy in the film is obtained by integrating through its volume,

$$E^{\text{film}} = \int_{-h/2}^{h/2}\int_{-\infty}^{\infty}\int_{-\infty}^{\infty}\frac{1}{2}C_{\alpha\beta\delta\gamma}\varepsilon^e_{\alpha\beta}\varepsilon^e_{\delta\gamma}dx_1dx_2dx_3. \tag{4}$$

Substituting Eq. (3) into Eq. (4) and integrating with respect to x_3 leads to

$$E^{\text{film}} = E^{\text{film}}_s + E^{\text{film}}_b, \tag{5}$$

where

$$E^{\text{film}}_s = \frac{1}{2}\int_{-\infty}^{\infty}\int_{-\infty}^{\infty}N_{\alpha\beta}e_{\alpha\beta}dx_1dx_2, \tag{6}$$

$$E^{\text{film}}_b = \frac{1}{2}\int_{-\infty}^{\infty}\int_{-\infty}^{\infty}D\left[(\Delta\zeta)^2 - 2(1-v_f)\left(\zeta_{,11}\zeta_{,22} - \zeta^2_{,12}\right)\right] \times dx_1dx_2, \tag{7}$$

$$e_{\alpha\beta} = \frac{1}{2}(u_{\alpha,\beta} + u_{\beta,\alpha}) + \frac{1}{2}\zeta_{,\alpha}\zeta_{,\beta} - \varepsilon^0_{\alpha\beta}, \tag{8}$$

$$N_{\alpha\beta} = \frac{2h\mu_f}{1-v_f}[(1-v_f)e_{\alpha\beta} + v_f e_{\gamma\gamma}\delta_{\alpha\beta}], \tag{9}$$

where $D = \frac{\mu_f h^3}{6(1-v_f)}$, $\Delta = \nabla\cdot\nabla$, and μ_f and v_f are the shear modulus and Poisson's ratio of the film, respectively. In the former system, the substrate is elastic, and the film is perfectly bonded to the substrate with a zero displacement jump across the interface between them ($\mathbf{u}^f = \mathbf{u}^s$). Given the substrate surface displacement u^s_i, the traction induced at the substrate surface is obtained using a Green's function method [24],

$$T^s_i = \frac{1}{(2\pi)^2}\int M_{ij}\tilde{u}^s_j e^{i\xi_\alpha x_\alpha}d\xi_1d\xi_2. \tag{10}$$

The elastic energy in the substrate $E^{\text{sub}} = \frac{1}{2}\int_{-\infty}^{\infty}\int_{-\infty}^{\infty}T^s_i u^s_i dx_1dx_2$ finally has the form

$$E^{\text{sub}} = \frac{1}{8\pi^2}\int M_{ij}\tilde{u}^f_i\tilde{u}^{f*}_j d\xi_1d\xi_2, \tag{11}$$

where the symbol * denotes the complex conjugate and M_{ij} is a matrix function of n_α. Therefore,

$$M_{ij} = \frac{\mu_s\xi}{3-4v_s}\begin{bmatrix} 4(1-v_s)-n_2^2 & n_1n_2 & 2i(1-2v_s)n_1 \\ n_1n_2 & 4(1-v_s)-n_1^2 & 2i(1-2v_s)n_2 \\ -2i(1-2v_s)n_1 & -2i(1-2v_s)n_2 & 4(1-v_s)\end{bmatrix}, \tag{12}$$

with μ_s and v_s as the shear modulus and Poisson's ratio of the substrate, respectively, and $\xi = (\xi_1^2+\xi_2^2)^{1/2}, n_1 = \xi_1/\xi, n_2 = \xi_2/\xi$. The total elastic energy of the film-substrate system $E^{\text{tot}} = E^{\text{film}} + E^{\text{sub}}$ can be expressed as a functional of the middle-plane displacement in the film. The stationary variation in the total elastic energy with respect to the middle-plane

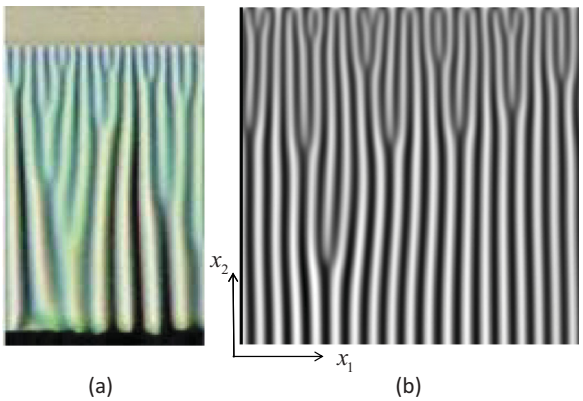

FIG. 4. (Color online) Comparison between (a) the observed hiearchical wrinkling pattern in Ref. [15] and (b) our simulated pattern.

displacement leads to the elastic equilibrium in the substrate, in-plane, and out-of-plane equilibrium equations in the film. $\delta E^{\text{tot}}/\delta u_\alpha = 0$ leads to the in-plane equilibrium equation of the film $N_{\alpha\beta,\beta} = T^s_\alpha$. When the stiffness inhomogeneity of the film is described by a positionally dependent shear modulus $\mu_f(x_1,x_2)$, solving the in-plane equilibrium equation reduces to the problem of the two-dimensional elastically heterogeneous solid of $\mu_f(x_1,x_2)$ containing arbitrary effective eigenstrain $\varepsilon^0_{\alpha\beta} - \frac{1}{2}\zeta_{,\alpha}\zeta_{,\beta}$. The solution can be obtained using the phase field microelasticity theory [29]. The out-of-plane equilibrium process is described using the time-dependent Ginzburg-Landau kinetic equation,

$$\frac{\partial \zeta}{\partial t} = -\Gamma \frac{\delta E^{\text{tot}}}{\delta \zeta}, \tag{13}$$

where Γ is a kinetic coefficient which characterizes the relaxation rate of the buckling process in the overdamped dynamics. The steady-state solution of Eq. (13) $\delta E^{\text{tot}}/\delta\zeta = 0$ recovers the out-of-plane equilibrium equation of the film $D(x_1,x_2)\Delta^2\zeta - (N_{\alpha\beta}\zeta_{,\alpha})_{,\beta} + T^s_3 = 0$ and provides the equilibrium distributions of ζ. Throughout the paper Greek indices are used to indicate 1 or 2, and Latin indices indicate 1,2 or 3. The usual summation convention applies for repeated indices, and a comma stands for differentiation with respect to the suffix index. A similar semi-implicit spectrum method [26] is adopted to solve Eq. (13) after Eqs. (6)–(12) are substituted into Eq. (13), the dimensional quantities are scaled by the film thickness ($r' = r/h$), and the time t is scaled by $\tau = h/\Gamma_\zeta \mu_s$ (i.e., $t' = t/\tau$). A square computational domain of size 1024 $\times$ 1024 is used with periodical boundary conditions and the time step $\Delta t' = 1$ (unless otherwise noted).

A simulated result in Fig. 4 shows that there is a hierarchical wrinkling pattern when the film of thickness h with a prescribed gradient stiffness, $\bar{E}_f(x_2) = \bar{E}^{(2)}_f[1 + (\alpha - 1)\frac{x_2}{N_2}]$, $\alpha = 0.1$, $N_2 = 1024$, $\lambda^e_2 = 20\pi h$, and $\varepsilon_c = (3\bar{E}_s/\bar{E}^{(2)}_f)^{2/3}/4$ is under a uniaxial compression $\varepsilon^0_{11} = \varepsilon_{\text{pre}} = 3\varepsilon_c$ along the x_1 axis. This hierarchical wrinkle pattern may be viewed as a result of the cascade instability of the wrinkle branching. The result in Fig. 4 is in striking agreement with the experimental observation of the hierarchical wrinkling pattern in the solvent-induced wrinkling of the multilayer system, wherein it is believed that solvent diffusion changes the glass transition temperature of the polymer film and results in a stiffness gradient in the film [15]. It is seen that the closer the diffusion front, the smaller the film stiffness and the smaller the wrinkle wavelength. This agreement confirms that the spontaneous wrinkle branching by the stiffness gradient in the film can produce a hierarchical wrinkling pattern. Therefore, we expect that the patterning stiffness gradient in the film could be an effective strategy to realize a controllable hierarchical wrinkling pattern. We can control the stiffness gradient of the film by regulation of binary composition modulation [30], gradient cross-linking density in a polymer film [31], or a hybrid nanocomposite [32,33].

When the stiffness gradient is from the substrate, its stiffness can be quantitatively controlled by the cross-linking density if the substrate is a cross-linked polymer [31]. We found that the stiffness gradient of the substrate can also be induced by the interplay between the substrate viscoelasticity and the diffusion process if the substrate is viscoelastic. It is known that the wrinkle in a compressively stressed film on a viscoelastic substrate undergoes a coarsening process [26,34]. The increase in the wrinkle wavelength during coarsening is corresponding to the decrease in the substrate stiffness due to stress-driven viscoelastic relaxation. When the compressive membrane stress in the film is caused by solvent diffusion mediated inhomogeneous swelling [27], the time- and spatial-dependent stresses transmitted into the substrate facilitate a nonuniform viscoelastic relaxation and, thus, lead to a dynamic stiffness gradient of the substrate. In this situation, the amplitude of the stiffness inhomogeneity in the substrate is characterized by the difference in the modulus at the glassy and rubbery states [34], whereas, the characteristic length of the stiffness inhomogeneity zone is dependent on the processes of viscous flow in the substrate and solvent diffusion in the film. To explore how and when a hierarchical wrinkling pattern in the film-substrate system can form due to such a stiffness gradient of the substrate, we modified the model [26] for kinetic wrinkling of a homogenous elastic film on a viscoelastic substrate by including the effect of solvent diffusion [27]. In the model, the elastic energy in the film is still given by Eqs. (5)–(9) after the eigenstrain is replaced by $\varepsilon^0_{ij} = \varepsilon^0\delta_{\alpha\beta}c(x_1,x_2,t)$ with ε^0 as a constant characterizing solvent-induced expansion and $c(x_1,x_2,t)$ as the solvent concentration. A thin-layer approximation of the linear viscoelastic response gives a relationship between the surface velocity and the traction of the viscoelastic layer with thickness H. The total energy dissipative process involves solvent diffusion, wrinkling in the film, and viscoelastic flow in the substrate. The process is described by a set of nonlinear evolution equations with respect to the middle-plane displacement of the film [26] and the solvent concentration [27],

$$\frac{\partial \zeta}{\partial t} = \frac{1-2\nu_s}{2(1-\nu_s)}\frac{H}{\eta}\left[-D\frac{\partial^4\zeta}{\partial x_\alpha\partial x_\alpha\partial x_\beta\partial x_\beta} + \frac{\partial N_{\alpha\beta}}{\partial x_\beta}\frac{\partial\zeta}{\partial x_\alpha} + N_{\alpha\beta}\frac{\partial^2\zeta}{\partial x_\alpha\partial x_\beta}\right] - \frac{\mu_R}{\eta}\zeta, \tag{14}$$

$$\frac{\partial u_\alpha}{\partial t} = \frac{H}{\eta}\frac{\partial N_{\alpha\beta}}{\partial x_\beta} - \frac{\mu_R}{\eta}u_\alpha, \tag{15}$$

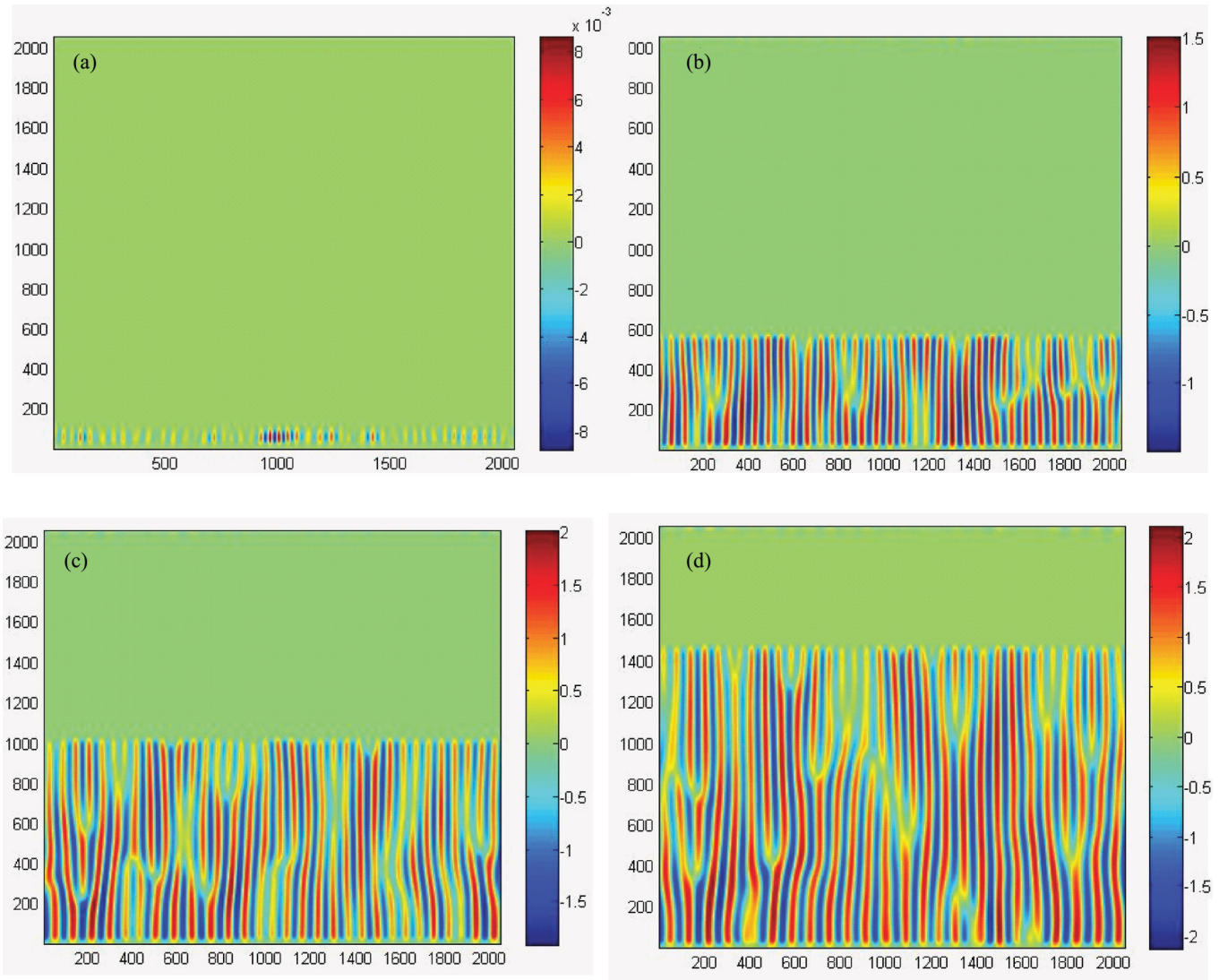

FIG. 5. (Color online) Simulated evolving wrinkling morphologies in the film-substrate system involve the viscous flow of the substrate and the unidirectional growth of the diffusion front (a)–(d) $t/\tau = 500$, 5000, 9500, and 14 000.

$$\frac{\partial c}{\partial t} = -\Gamma_c \left(\frac{\partial f}{\partial c} - 2\beta_c \nabla^2 c \right), \tag{16}$$

where η and μ_R are the viscosity and the rubbery modulus of the viscoelastic substrate. $f(c,a) = A[\frac{1}{4}c^4 - (\frac{1}{2} - \frac{1}{3}\chi)c^3 + (\frac{1}{4} - \frac{1}{2}\chi)c^2]$ is a chemical potential describing solvent diffusion controlled domain growth with A as a constant and $\chi > 0$ for the growth of the diffusion front. Γ_c is the related diffusion mobility coefficient, and β_c is the gradient coefficient. We followed the numerical procedure [26,27] to solve Eqs. (14)–(16).

Figure 5 shows the simulated sequential wrinkling morphologies during the film-substrate system, which involves the viscous flow of the substrate and the unidirectional growth of the diffusion front. The chosen parameters are $h = 1$, $H = 10$, $\nu_f = 0.3$, $\nu_s = 0.45$, $\mu_f = 1$, $\mu_R = 0$, $\varepsilon^0 = 0.003$, $\chi = 0.1$, $\rho = A/\mu_f = 6$, and $\xi = \frac{2\beta_c}{\mu_f h_f^2} = 1$. Figure 5(a) demonstrates that parallel wrinkles tend to form behind the area of the diffusion front with the alignment perpendicular to the direction of maximum compression [27]. After the characteristic length of the substrate inhomogeneity zone becomes larger than a critical value, the wrinkle-branching instability occurs as shown in Fig. 5(b). With the further propagation of the diffusion front, the cascade branching of the wrinkle develops, and finally, a hierarchical wrinkling pattern forms. Figure 6 shows that the simulated wrinkling morphological evolution during the film-substrate system involves the viscous flow of the substrate and the radial growth of the diffusion front with the same input parameters as in Fig. 5. The wrinkling pattern tends to arrange into a radial hierarchical stripe pattern. The wrinkling pattern has a smaller wavelength at the circular diffusion front and a larger wavelength away from the diffusion front with multiple wrinkle branchings bridging them. The wrinkling pattern obtained in the current simulation is significantly different from other solvent-induced wrinkling of multilayer systems [35], wherein few wrinkle branchings are observed due to the lack of the stiffness gradient.

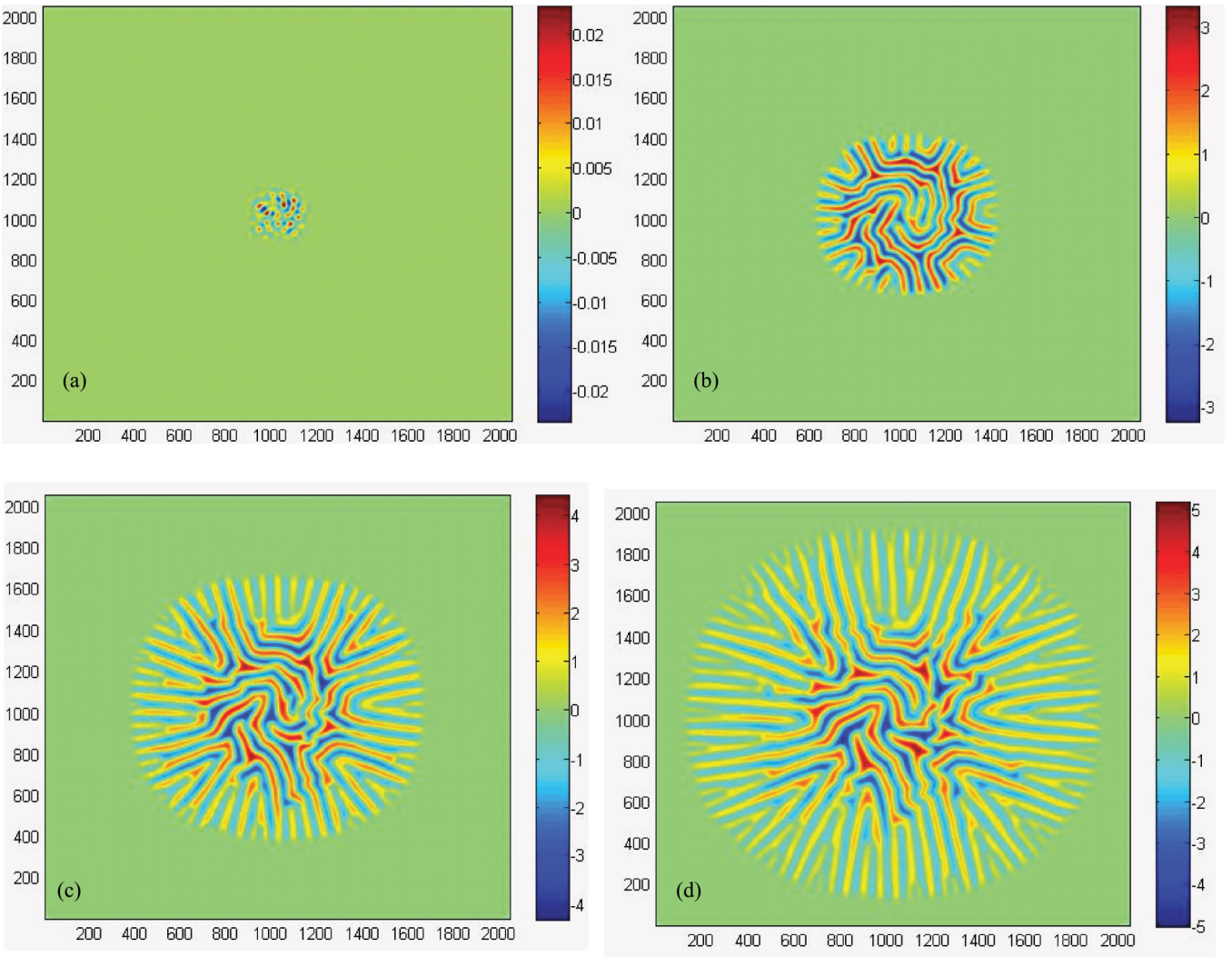

FIG. 6. (Color online) Simulated evolving wrinkling morphologies in the film-substrate system involve the viscous flow of the substrate and the radial growth of the diffusion front (a)–(d) $t/\tau = 500$, 3500, 5500, and 8000.

We can estimate that the characteristic length of the stiffness inhomogeneity zone is on the order of $L/h \sim \Gamma_c \eta$ in the film-substrate system involving the viscous flow in the substrate and solvent diffusion in the film. The wrinkle-branching instability that results in the hierarchical wrinkling pattern occurs as the critical condition $\Gamma_c \eta > L_c/h$ is satisfied. Obviously, large values of the diffusion mobility Γ_c and the substrate viscosity η are found to facilitate formation of the hierarchical wrinkling pattern. We found that a phase diagram for the morphology of such a film-substrate system under supercritical compression can be constructed in the space with $\Gamma_c' = \Gamma_c \mu_f \tau$ and $1/\eta' = \tau \sigma_0^2/\mu_f \eta$ as the coordinates as shown in Fig. 7, wherein the boundary curve $\Gamma_c' = F/\eta'$ with F as a constant separating the buckling morphology of the film in a uniform straight wrinkle state or in a wrinkle-branching state. By using a set of numerical simulations, the transition from the uniform straight wrinkle state to the wrinkle-branching state can be identified by tracking the configuration instability of the film-substrate system for various cases with different values of these Γ_c''s and η''s. The result in Fig. 7 shows that the simulated transition points are collapsed into the curve $\Gamma_c' = F/\eta'$ in good agreement with our analysis. The obtained phase diagram here may be used to guide formation of the hierarchical

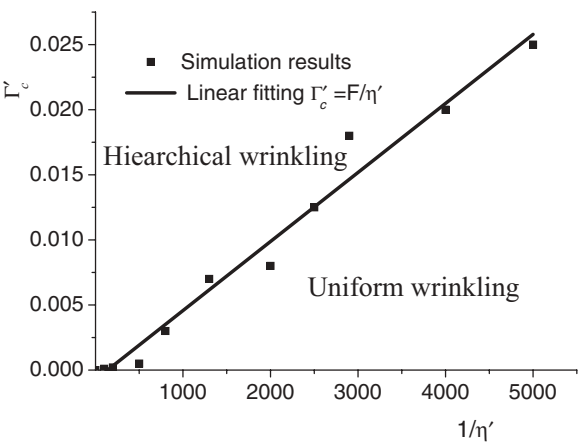

FIG. 7. The calculated phase diagram for the wrinkle branching coupled to diffusion of the film on a viscoelastic substrate constructed in the space with Γ_c' and $1/\eta'$ as the coordinates.

wrinkling pattern for a film on the viscoelastic substrate by tuning the properties of viscous flow in the substrate and solvent diffusion in the film.

IV. CONCLUSIONS

To summarize, the mechanism of the wrinkle-branching instability, leading to formation of the hierarchical wrinkling pattern in compressed film-substrate systems, was revealed. The critical conditions for the spontaneous wrinkle-branching instability by the stiffness gradient were identified. The wrinkle-branching instability, as the coherency loss of domains, occurred when the characteristic length of the stiffness inhomogeneity zone was larger than the coherency persistent length. The numerical simulations confirmed the theoretic analysis and revealed formation of the hierarchical wrinkle pattern in two film-substrate systems. The results obtained in the paper may be of interest in engineering complex wrinkling patterns in the film-substrate system by regulation of the stiffness gradient.

ACKNOWLEDGMENTS

This work was supported by the Basic Research Program of China (Grants No. 2010CB934700 and No. 2011CB302100) and the Chinese Natural Science Foundation (Grants No. 11072232 and No. 11132009). Y. Ni also gratefully appreciates the financial support from the "Hundred of Talents Project" of the Chinese Academy of Sciences.

[1] R. V. Kohn and S. Müller, Philos. Mag. A **66**, 697 (1992).
[2] A. Saxena, Y. Wu, T. Lookman, S. R. Shenoy, and A. R. Bishop, Physica A **239**, 18 (1997).
[3] B. Li and M. Luskin, Mater. Sci. Eng. A **273**, 237 (1999).
[4] S. Kaufmann, R. Niemann, T. Thersleff, U. K. Rößler, O. Heczko, J. Buschbeck, B. Holzapfel, L. Schultz, and S. Fähler, New J. Phys. **13**, 053029 (2011).
[5] J. C. Loudet, P. V. Dolganov, P. Patricio, H. Saadaoui, and P. Cluzeau, Phys. Rev. Lett. **106**, 117802 (2011).
[6] A. S. Argon, V. Gupta, H. S. Landis, and J. A. Cornie, J. Mater. Sci. **24**, 1207 (1989).
[7] M. Ortiz and G. Gioia, J. Mech. Phys. Solids **42**, 531 (1994).
[8] S. Conti, A. DeSimone, and S. Müller, Comput. Methods Appl. Mech. Eng. **194**, 2534 (2005).
[9] F. Brau, H. Vandeparre, A. Sabbah, C. Poulard, A. Boudaoud, and P. Damman, Nat. Phys. **7**, 56 (2010).
[10] D. P. Holmes and A. J. Crosby, Phys. Rev. Lett. **105**, 038303 (2010).
[11] P. Kim, M. Abkarian, and H. A. Stone, Nature Mater. **10**, 952 (2011).
[12] J. S. Huang, B. Davidovitch, C. D. Santangelo, T. R. Russell, and N. Menon, Phys. Rev. Lett. **105**, 038302 (2010).
[13] H. Vandeparre, M. Pineirua, F. Brau, B. Roman, J. Bico, C. Gay, W. Bao, C. N. Lau, P. M. Reis, and P. Damman, Phys. Rev. Lett. **106**, 224301 (2011).
[14] R. D. Schroll, E. Katifori, and B. Davidovitch, Phys. Rev. Lett. **106**, 074301(2011).
[15] H. Vandeparre, S. Gabriele, F. Brau, C. Gay, K. K. Parker, and P. Damman, Soft Matter **6**, 5751 (2010).
[16] J. Yin and X. Chen, Philos. Mag. Lett. **90**, 423 (2010).
[17] A. L. Roitburd, Solid State Phys. **33**, 317 (1978).
[18] A. G. Khachaturyan, *Theory of Structural Transformations in Solids* (Wiley, New York, 1983).
[19] J. A. Rogers, T. Someya, and Y. G. Huang, Science **327**, 1603 (2010).
[20] K. Efimenko, M. Rackaitis, E. Manias, A. Vaziri, L. Mahadevan, and J. Genzer, Nature Mater. **4**, 293 (2005).
[21] H. G. Allen, *Analysis and Design of Structural Sandwich Panels* (Pergamon, New York, 1969).
[22] J. Groenewold, Physica A **298**, 32 (2001).
[23] E. Cerda and L. Mahadevan, Phys. Rev. Lett. **90**, 074302 (2003).
[24] Z. Y. Huang, W. Hong, and Z. Suo, J. Mech. Phys. Solids **53**, 2101 (2005).
[25] J. W. Cahn and J. E. Hilliard, J. Chem. Phys. **28**, 258 (1958).
[26] R. Huang and S. H. Im, Phys. Rev. E **74**, 026214 (2006).
[27] Y. Ni, L. H. He, and Q. Liu, Phys. Rev. E **84**, 051604 (2011).
[28] E. H. Mansfield, *The Bending and Stretching of Plates*, 2nd ed. (Cambridge University Press, Cambridge, UK, 1989).
[29] Y. U. Wang, Y. M. Jin, and A. G. Khachaturyan, J. Appl. Phys. **92**, 1351 (2002).
[30] C. Y. Jiang, S. Singamaneni, E. Merrick, and V. V. Tsukruk, Nano Lett. **6**, 2254 (2006).
[31] M. Guvendiren, S. Yang, and J. A. Burdick, Adv. Funct. Mater. **19**, 3038 (2009).
[32] T. R. Hendricks, W. Wang, and I. Lee, Soft Matter **6**, 3701 (2010).
[33] J. W. Liu, J. Xu, Y. Ni, F. J. Fan, C. L. Zhang, and S. H. Yu, ACS Nano **6**, 4500 (2012).
[34] R. Huang, J. Mech. Phys. Solids **53**, 63 (2005).
[35] H. Vandeparre and P. Damman, Phys. Rev. Lett. **101**, 124301 (2008).